Investigation of Channel Reciprocity for OFDM TDD Systems

by

Senay Haile

A thesis
presented to the University of Waterloo
in fulfillment of the
thesis requirement for the degree of
Master of Applied Science
in
Electrical and Computer Engineering

Waterloo, Ontario, Canada, 2009

I hereby declare that I am the sole author of this thesis. This is a true copy of the thesis, including any required final revisions, as accepted by my examiners.

I understand that my thesis may be made electronically available to the public.

Senay Haile

Abstract

This dissertation investigates the assumption of channel reciprocity in orthogonal frequency division multiplexing (OFDM) systems using time-division duplex (TDD) access. Within TDD systems uplink and downlink transmission share the same channel, and so channel state at the transmitter (CSIT) can be inherently obtained through uplink channel estimation assuming that the channel is reciprocal and static over a few packet transmissions. For both closed-loop SISO-OFDM (single-input single-output) and MIMO-OFDM (multiple-input multiple-output) systems, the availability of CSIT enables the transmitter to apply adaptive modulation and coding (AMC) to improve throughput or signal processing and precoding algorithms in order to obtain a spatial diversity and/or multiplexing gain. This results in improved performance as compared to open-loop MIMO systems in which the channel state is not known at the transmitter. However, significant deviations between transmitter and receiver channel state information may result in degradation of performance, as precoding at the transmitter will be based on erroneous channel state information. In this work, we observe the assumption of channel reciprocity using a real-time OFDM-PHY FPGA prototype wireless communications system and we look at possible factors that contribute to deviations between uplink and downlink channel estimates. We also look at common linear precoding schemes to compensate for channel non-reciprocity. Of all the possible factors that contribute to channel reciprocity deviations, we find that the dominant factor comes from imperfections in the RF front-end components which result in significant channel phase response deviations across subcarriers between the uplink and downlink.

Acknowledgments

I would like to thank my supervisor, Prof. Amir K. Khandani, for his guidance throughout my graduate studies. His deep knowledge on the subject matter and willingness to provide his graduate students with state-of-the-art lab equipment and hardware has been very valuable. Also, I would like to thanks my colleagues and friends, namely Jake, Arijit and Felix for their memorable discussions and laughs throughout my studies.

Lastly and foremost I would like to thank my parents, Haile Ogbaldet and Nigisti Ghebrezgiher, as well as my brother Nerayo and sisters Rahwa and Salam for their support and belief in me.

Contents

List of Figures

Chapter 1

Introduction

With the advent of ubiquitous and high bandwidth mobile access, mobile operators are looking at 4G mobile technology to provide the high data-rates needed to support the growing number of multimedia functions featured on mobile terminals. The underlying physical layer algorithms utilized in next generation mobile technology, such as WiMax and LTE, are Orthogonal Frequency Division Multiplexing (OFDM) and Multiple-Input Multiple-Output technology (MIMO). The high spectral efficiency and relative immunity to intersymbol interference (ISI) of OFDM, as well as its' ability to convert a frequency-selective channel into a set of frequency-flat subchannels deem it as an excellent choice for fading and scattering mobile channels. Furthermore, the emergence of MIMO technology allows for the presence of spatial channels within rich-scattering mobile channels. These independent spatial channels allow for exploitation of spatial diversity or increased capacity by transmitting on these separate spatial channels using the same subcarriers and time slots.

Both WiMax and LTE standards allow for channel access based on Time-Division Du-

plex (TDD), which means that downlink and uplink transmission between the basestation and mobile terminals will share the same frequency spectrum and requires a fairly sophisticated Medium Access Control (MAC) protocol to ensure optimum sharing of the spectrum. This is in contrast to Frequency Division Duplex, also supported by both standards for compliance with regulatory pairing requirements [4], in which uplink and downlink transmission can occur simultaneously on separate spectrums. There are several advantages to using TDD channel access for MIMO-OFDM systems. These include more efficient use of spectrum, less complex transveiver designs, flexibility in choosing uplink-to-downnlink data-rate ratios, and exploitation of channel reciprocity [3]. It specifically is the exploitation of channel reciprocity that allows for the efficient implementation of various SISO and MIMO-based transmission schemes which serve to improve throughput and spectral usage, exploit diversity and improve capacity.

1.1 Applications of Channel Reciprocity

Channel reciprocity can theoretically be assumed for channels in which uplink and downlink transmission share the same frequency spectrum and when the coherence time of the channel is much greater than the OFDM packet period. This is usually true for channels with low Doppler spread, as characterized by the channel models described in the 802.11a/g/n standards [2, 3]. This assumption means that the uplink terminal (i.e. basestation) can acquire knowledge of the channel just through uplink channel estimation. This is referred to as Channel State Information at the Transmitter (CSIT). Several transmission schemes rely on full or partial CSIT in order to operate properly, and some of these will be discussed.

For SISO-OFDM systems, the transmission scheme that benefits the most from CSIT is Adaptive Modulation and Coding (AMC). This is a standard feature in the WiMax standard [4]. In AMC transmission, the transmitter chooses the modulation scheme and channel coding parameters based on the received signal-to-noise ratio (SNR) which is heavily dependent on the channel magnitude, all with respect to individual subcarriers. For subcarriers with relatively strong channel magnitudes a higher order modulation scheme (i.e. 16/64 QAM) and coding rate (4/5, 5/6) can be used to improve throughput. Correspondingly, for subcarriers with relatively weak channel magnitudes a lower modulation (BPSK, QPSK) and coding rate (1/2, 2/3) can be used to increase resiliency for bad channel conditions. Research has shown this type of transmission scheme can dramatically increase the throughput and improve immunity to bad channel conditions [7].

For MISO-OFDM systems in which the basestation contains multiple antennas and the mobile terminal contains a single antenna, an effective transmission scheme utilizing CSIT that serves to improve received SNR and increase resilience to fading conditions is transmit beamforming [19], also known as Maximuim Ratio Combining at the Transmitter (MRT). In MRT, the same symbol is transmitted across all antennas. Before transmission, the symbol is weighed per antenna according to the conjugated complex channel coefficient per subcarrier that was estimated in the previous uplink transmission. For OFDM systems the channel impulse response can be represented in the frequency domain by a multiplicative complex channel coefficient per subcarrier due to the orthogonality of the subcarriers that comprise an OFDM symbol and by the usage of the cyclic prefix (CP) which converts a discrete convolution in the time domain into a scalar multiplication. By weighing the symbol per antenna with the conjugated complex channel coefficient per tone

and presuming that the channel is static over multiple packet transmissions, in effect the complex channel coefficient applied by the channel can be compensated for by the conjugated complex weight. This leads to coherent reception in terms of phase as seen by the mobile terminal, which maximizes the SNR at the receiver. For this transmission to be effective it is imperative that the transmitter possesses accurate knowledge of the channel and specifically the channel phase per tone per antenna.

For MIMO-OFDM systems in which the basestation contains multiple antennas and the mobile terminal either contains multiple antennas or several mobile terminals each contain a single antenna, an effective transmission scheme utilizing CSIT to improve data rates or capacity is referred to as spatial multiplexing, of which one scheme is Singular Value Decomposition (SVD). This scheme is effective in rich-scattering multipath environments such that the physical paths between the Tx and Rx antennas are uncorrelated with each other. In these types of environments, where the number of possible spatial paths is the lower of Nr, Nt, the channel can be represented by a N_rxN_t matrix per subcarrier where N_r is the number of receive antennas and N_t is the number of transmit antennas. The channel matrix can be decomposed using SVD or other types of decomposition methods such that it can be represented by eigenvectors and eigenvalues, and will ideally have a rank equal to the lower of N_r, N_t. Precoding at the transmitter can be achieved using the eigenvectors of the factorized channel matrix. Power allocation per subcarrier across the spatial streams are based on the eigenvalues of the channel matrix, and can be distributed using the classical water-filling method [8]. WIth precoding, the effects of the channel on the transmitted data can be compensated and what results is the N_tx1 transmit data matrix is multiplied by a quasi-identity matrix which arrives at each receive antenna in its

original form, thus allowing for multiple data streams to be transmitted simultaneously. However, in order for this to properly function it is absolutely imperative that CSIT at the transmitter is accurate. Errors in CSIT can result in multi-data stream or multi-user interference which leads to excessive bit error rates.

1.2 Contributions of Thesis

This thesis focuses on the validity of channel reciprocity within OFDM TDD systems. After looking at possible factors that contribute to non-reciprocity, we look at a few methods to compensate for and overcome non-reciprocity. Furthermore, we observe channel reciprocity within a real-time hardware platform and analyze the results. The results show that though the channel magnitude across tones and time is in fact reciprocal, there exists deviations between uplink and downlink channel phase across tones that can be attributed to RF impairments. We then look at a simple way to compensate for phase deviations using an adaptive linear precoding algorithm.

1.3 Organization of Thesis

The remainder of this thesis is organized as follows. In Chapter 2, the factors that affect non-reciprocity are examined with respect to the OFDM system model. In Chapter 3, some common methods for alleviating channel non-reciprocity are described. In Chapter 4, the hardware setup in which channel reciprocity is tested is described. In addition to the experiment description, the findings are analyzed. Lastly, conclusions and future research are presented in Chapter 5.

Chapter 2

Factors that Contribute to Channel Non-Reciprocity

In order to examine the factors that contribute to the deterioration of channel reciprocity, it is imperative that an effective OFDM system model is created in which the inherent factors are addressed. After the OFDM system model is described, then factors of channel non-reciprocity to the OFDM TDD system model are explained. Though the following model represents a SISO OFDM chain, it can be extended to multiple OFDM chains in the case of MIMO mode. The impairments described are compounded in MIMO systems.

2.1 OFDM System Model

As stated before, the advantages that OFDM offers lies with its high spectral efficiency achieved by its overlapping and independent subcarriers, its ability to convert a frequency-selective channel into a set of frequency-flat subchannels and its relatively long symbol time

which counteracts the effects of ISI caused by multipath [17]. However, OFDM suffers from sensitivity to timing and carrier frequency offsets, as well as its dependency on costly power amplifiers with high peak-to-average power ratio (PAPR). A block diagram of the OFDM system is in Figure 2.1.

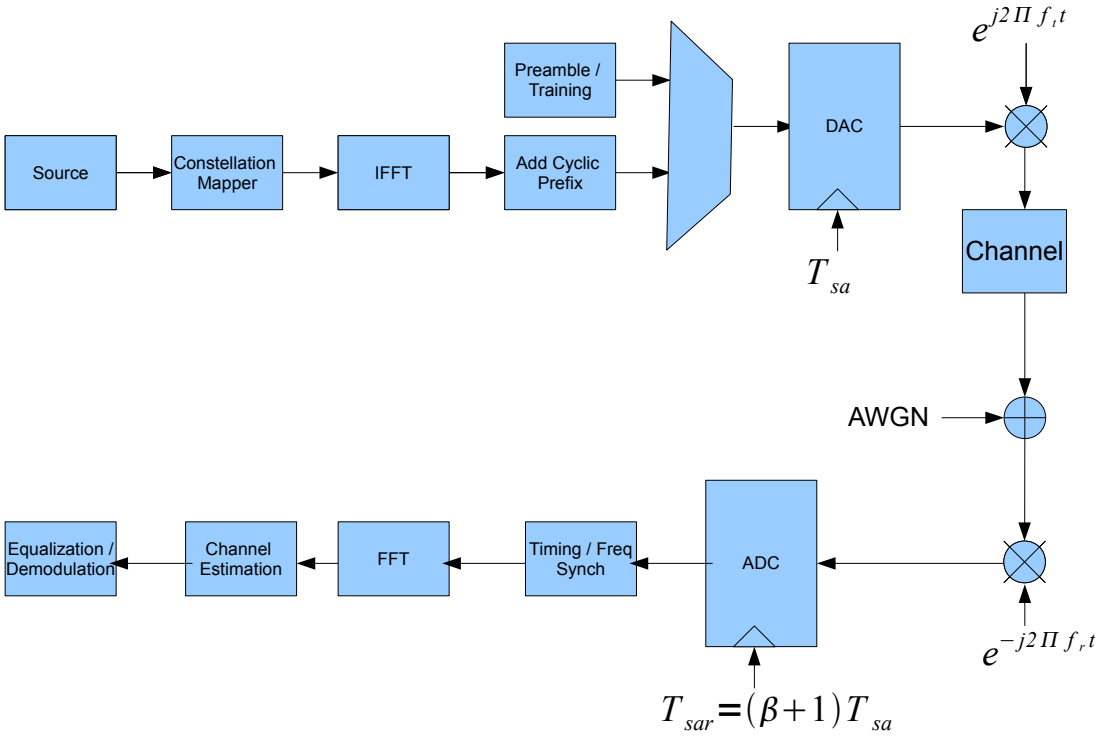

Figure 2.1: OFDM System Model

At the transmitter a group of N data symbols are mapped into N complex QAM symbols, which are then fed into the IFFT block to produce one OFDM symbol in the time-domain. It can be represented by the following equation.

$$s_b(t) = \sum_{k=0}^{N-1} S_k e^{j2\pi f_k t}, \quad 0 \leq k \leq N-1 \tag{2.1}$$

where S_k is the complex symbol at the kth subcarrier and $f_k = k\triangle(f) = k/F_s$ is the subcarrier spacing. If $s_b(t)$ is sampled at an interval of $T_{sa} = T_s/N$, where T_s is the OFDM symbol period, T_{sa} is the sampling period and N is the number of subcarriers then the sampled baseband symbol can be represented by the following equation.

$$s_b(nT_s/N) = \sum_{k=0}^{N-1} S_k e^{j2\pi f_k nT_s/N}, \quad 0 \leq k \leq N-1 \tag{2.2}$$

$$s_b[n] = \sum_{k=0}^{N-1} S_k e^{j2\pi kn/N}, \quad 0 \leq k \leq N-1 \tag{2.3}$$

$$s_b[n] = IFFT_N \{S_k\} \tag{2.4}$$

In equation (2.4) n is the time domain sampling index and $k = f_k T_s$ is the subcarrier index $k = f_k T_s$. Following the IFFT block, a cyclic prefix (CP) of sample length N_G is inserted into the start of each OFDM symbol. The purpose of the CP is to counter the effects of ISI in the multipath channel and simplify equalization at the receiver, and the length of the CP is chosen to be greater than the maximum channel delay spread in samples.

After the IFFT block and CP insertion, the OFDM symbol is then fed into the digital-to-analog (DAC) converter where it is converted to a continuous time-domain signal $x_b(t)$. Afterwards, it is filtered by a low-pass filter with bandwidth $1/T_s$ where $F_s = 1/T_s$ is the

Nyquist rate of the OFDM symbol with sampling period T_s. It is then upconverted to the transmitter carrier frequency f_{ct} and amplified before transmission. Equation (2.6) represents the OFDM passband symbol.

$$\begin{aligned} s_p(t) &= Re\left\{s_b(t)e^{j2\pi f_{ct}t}\right\} && (2.5) \\ &= s_I(t)cos(2\pi f_{ct}t) - s_Q(t)sin(2\pi f_{ct}t) && (2.6) \end{aligned}$$

Furthermore, the channel in which the signal traverses through can be described as a channel with multipath delay spread and additive complex AWGN noise. The channel is assumed to have maximum delay spread τ_{max} less than the cyclic prefix time T_g, and the additive noise $n(t)$ can be described by Independent Identically Distributed (IID) complex zero-mean Gaussian noise with variance σ_n^2. In addition, the channel can be modeled at the baseband with no loss of generality. The following equation describes how the transmitted signal is distorted by the channel.

$$x(t) = \sum_i \gamma_i \bar{s}(t, \tau - \tau_i) + n(t) \quad (2.7)$$

The gain and delay of each path i in the multipath channel is described by γ_i and τ_i respectively. Assuming perfect frequency offset and sampling clock estimation at the receiver, and neglecting the complex AWGN component of the channel, the demodulated signal can be described by the following equation, which is analogous to the DFT at the receiver.

$$
\begin{aligned}
X_m &= (1/T_s)\int_0^{T_s} x(t)e^{-j2\pi f_m t}dt && (2.8)\\
&= \sum_i \gamma_i 1/T_s \int_0^{T_s} \bar{s}(t,\tau-\tau_i)e^{-j2\pi f_m t}dt + n(t) && (2.9)\\
&= \sum_i \gamma_i s_m e^{-j2\pi f_m \tau_i} + n(t) && (2.10)\\
&= H(f_m)e^{-j2\pi f_m \tau} s_m + n(t) && (2.11)
\end{aligned}
$$

where $H(f) = \sum_i \gamma_i e^{-j2\pi f \tau_i}$ is the frequency response of the multipath channel [17]. The received symbol is the original symbol with a phase shift by a sub-carrier dependent timing offset and a multiplicative component dependent on the channel frequency response at that subcarrier, along with complex AWGN. This greatly simplifies equalization, in which complex division can compensate for the multipath distortion if the channel coefficient for the given subcarrier is known.

At the receiver the signal is amplified, down-converted to baseband and low-pass filtered before entering the analog-to-digital converter (ADC). When the signal is down-converted, it is multiplied by a quadrature mixer with receive carrier frequency f_{cr}. The receive carrier frequency usually differs from the transmit carrier frequency f_{ct} due to drift and error tolerances on the local oscillators (LO) from which the carrier frequency is derived using a phase locked loop (PLL). Furthermore, at the ADC the received signal is sampled at sampling period $T_{sar} = (\beta + 1)T_{sa}$ which differs from the transmit sampling period T_{sa} due to phase noise from the LO and will be described later in this chapter. If the transmitted signal is transmitted at $t = 0$, the received signal $y(t)$ can be seen anywhere from time frame $t = t_o + T_h$ to $t = t_o + T_g + T_s$ where t_o is the timing offset and can be

described by the following equation. The equation incorporates the effects of the channel (H_k), carrier frequency offset ($\delta_f = f_{ct} - f_{cr}$) and timing offset ($t_o$).

$$y(t) = \sum_{k=0}^{N-1} H_k s_k e^{j2\pi(k\triangle f+\delta_f)(t-T_g-t_o)} + n(t) \tag{2.12}$$

$$y_n = y(nT_s/N) = \sum_{k=0}^{N-1} H_k s_k e^{j2\pi(k+k_o+\epsilon)(n-N_g-\theta_t)} + n_n \tag{2.13}$$

where $n \in [\theta_t + \nu, \theta_t + N + N_g]$, $\theta_t = t_0/T_s N$ is the integer offset in the OFDM frame, N_g is the number of samples of the cyclic prefix, $\nu = T_h/T_s N$ is the length of the channel in samples, and k_o and ϵ are the integer and fractional frequency offsets respectively [17].

2.2 Detriments to Channel Reciprocity

As shown in the previous section, therein lies various impediments to channel non-reciprocity within the RF and baseband signal chain. The main impediments are examined and modelled in the next few headings.

2.2.1 Carrier Frequency Offset

The frequency offset caused by carrier frequency differences at the transmitter and receiver has a direct effect on the demodulated OFDM symbol. Consider the following baseband OFDM symbol.

$$s(t) = \sum_k s_k e^{j2\pi f_k t} \tag{2.14}$$

Ignoring the effects of the channel and other impairments, the received OFDM symbol $x(t)$ will be distorted by frequency offset $\delta_f = f_{ct} - f_{cr}$.

$$x(t) = e^{j2\pi\delta_f t} s(t) \tag{2.15}$$

$$= e^{j2\pi\alpha\triangle f t} s(t) \tag{2.16}$$

where δ_f can take the form $\delta_f = \alpha\triangle f$. For demodulation, an integration (analogous to the DFT) is done for the sake of simplicity. The demodulated symbol X_m will take the form

$$X_m = (1/T_s) \int_0^{T_s} x(t) e^{-j2\pi f_m t} dt \tag{2.17}$$

$$= 1/T_s \int_0^{T_s} \sum_k e^{j2\pi\alpha\triangle f t} e^{-j2\pi(f_m - f_k)t} dt s_k \tag{2.18}$$

$$= \sum_k 1/T_s e^{j2\pi\alpha\triangle f t} \int_0^{T_s} s_k e^{-j2\pi(f_m - f_k)t} dt \tag{2.19}$$

$$= a_0 s_m + \sum_{k \neq m} a_{m-k} s_k \tag{2.20}$$

where a_l is defined as

$$a_l = 1/T_s \int_0^{T_s} e^{-j2\pi\alpha\triangle ft} e^{-j2\pi l\triangle ft} dt \quad (2.21)$$

$$= (sin[\pi(l-\alpha)]/\pi(l-\alpha)) e^{-j\pi(l-\alpha)} \quad (2.22)$$

$$= (-sin[\pi\alpha]/\pi(l-\alpha)) e^{-j\pi\alpha} \quad (2.23)$$

Depending on the value of α which can be represented as $\alpha = k_o + \epsilon$, where k_o is a whole number whereas ϵ is a fractional number with magnitude less than 1/2, significant phase distortion and/or attenuation can occur. Subcarrier integer shifts can occur for $k_o \neq 0$ and substantial inter-carrier interference (ICI) can occur for $\epsilon \geq 1/2$ [17].

2.2.2 Timing Offset

As shown in Equation (2.11), with the proper selection of CP length and neglecting other impairments a phase shift due to timing offset is induced into the demodulated symbol X_m. It takes the form $X_m = s_m e^{j2\pi f_m \tau}$ where τ represents the timing offset. The absence of the CP, or an insufficient CP length, can lead to additive interference from adjacent symbols.

2.2.3 Sampling Clock Deviations

The sampling clock rate between the transmitter and receiver usually differs due to LO jitter and phase noise, and this leads to degradation in peformance which become more pronounced over time [17]. As shown in 2.1, if the sampling clock period at the transmitter is $T_{sat} = T_{sa}$, then the sampling clock period at the receiver can be modelled as $T_{sar} =$

$(1+\beta)T_{sa}$. Without the sampling clock deviation the OFDM symbol can be demodulated by performing the DFT on $s(nT_s) = \sum_{k=0}^{N-1} s_k e^{j2\pi f_k nT_s}$ using a sampling period of T_{sa}. However, with the sampling clock offset at the receiver the samples will be $s(nT_{sar})_{n=0}^{N-1}$. When the DFT is applied to the sampled OFDM symbol with samling period T_{sar} at the receiver the demodulated symbol will take the form

$$X_m = (1/N)\sum_{n=0}^{N-1} s(nT_{sar})e^{-j2\pi nm/N} \tag{2.24}$$

$$= a_{m,m}s_m + \sum_{k\neq m} a_{m,k}s_k \tag{2.25}$$

where

$$a_{m,k} = sin[\pi(k-m+\beta k)]/Nsin(\pi/N(k-m+\beta k))e^{-j\pi((N-1)/N)(k-m+\beta k)} \tag{2.26}$$

From Equation (2.25) the demodulated symbol consists of the desired symbol s_m and ICI. Assuming that $N \gg 1$ and $\beta N \ll 1$, the desired symbol is modified by

$$a_{m,m} = (sin(\pi\beta m)/Nsin(\pi/N\beta m))e^{-j\pi((N-1)/N)\beta m} \tag{2.27}$$

$$\approx e^{-j\pi\beta M} \tag{2.28}$$

which is a subcarrier-dependent phase change [17].

2.2.4 Other Detriments

Although these following effects are not covered in this thesis, they will be briefly mentioned due to the ongoing research efforts attempting to understand and mitigate these

impairments. These include interference and correlation structures at the transmitter and receiver antennaes, as well as Doppler shifts relating to a time-varying channel.

Narrowband interference at either the transmitter or receiver terminal will lead to additive interference at subcarriers in which the interference is transmitted, causing channel estimation errors and ultimately channel non-reciprocity. There exists a number of ways to compensate for this, the most popular way being a feed-back loop to convey frame error rate (or similar metric) information to the transmitter in order to update modulation, transmit power and coding parameters as examined in [30]. Furthermore, correlation between antennaes which are spaced closer than the minimum distance needed to achieve physical independence play a role in channel non-reciprocity as well in MIMO systems. The covariance matrices representing the correlation between receiver/transmitter antennaes contribute to the overall channel response, and hence differing covariance matrices between transmitter and receiver terminals lead to channel estimation deviations and degrade reciprcority.

Doppler shift as attributed to a channel with a coherence time shorter than the OFDM packet period will cause frequency shifts in the received OFDM symbol which will affect performance and impair channel reciprocity. Unlike frequency offsets caused by carrier frequency differences, doppler shifts are not deterministic and depend on transmitter/receiver mobility aa well as the statistics of the channel. Furthermore, a time-varying channel may cause uplink channel estimates to be outdated in the sense that the downlink channel estimates were calculated at a prior time greater than the channel coherence time. As outlined in [16], sophisticated preamble and pilot structures need to be created in order to counter these effects.

As will be explained in Chapter 4, the channel is near-static throughout the setup and experiment so Doppler shifts are not a factor to channel non-reciprocity. Furthermore, external interference from narrowband devices (i.e. Bluetooth) are not present within the experiment.

Chapter 3

Compensating for Channel Non-Reciprocity

Compensation for non-reciprocity generally consists of obtaining correction factors derived from the frequency response per subcarrier of the transceiver circuitry. In effect, obtaining the frequency response per subcarrier of the transceiver can lead to precoding or application of a multiplicative correction factor which can counter the effects the transceiver imposes on the transmitted signal. Furthermore it can be shown that for the terminal requiring CSIT (i.e. basestation) for precoding, obtaining the transceiver frequency response at that terminal is sufficient for maintaining channel reciprocity, especially for MIMO systems. In other words the transceiver frequency response of the downlink terminal (i.e. mobile terminal) is not required for maintaining reciprocity.

Figure (3.1) presents the concatenated wireless channel plus radio channel between Station A (i.e. basestatiom) and Station B (i.e. mobile). In the figure $\boldsymbol{H_k^T}$ and $\boldsymbol{H_k}$ represent the reciprocal N_BxN_A downlink and N_AxN_B uplink channel per subcarrier k,

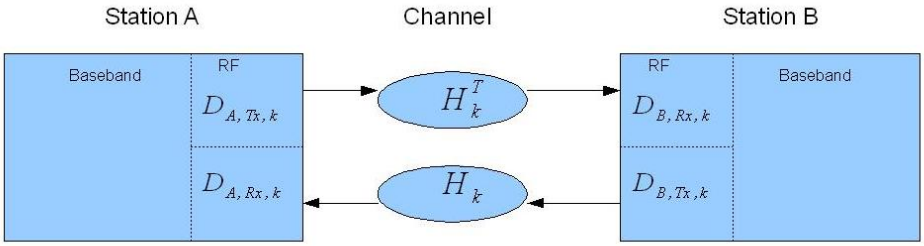

Figure 3.1: Equivalent Baseband-to-Baseband Channel

where N_A is the number of antennas at Station A and N_B is the number of antennas at Station B. The reciprocal channels are merely transposes of each other. Furthermore, $\boldsymbol{D_{A,Tx,k}}$ and $\boldsymbol{D_{A,Rx,k}}$ represent the N_AxN_A transmit and receive RF frequency response diagonal matrices per subcarrier k of Station A. The same goes for $\boldsymbol{D_{B,Tx,k}}$ and $\boldsymbol{D_{B,Rx,k}}$ for Station B, but with dimension N_BxN_B. In the uplink channel, the received signal at subcarrier k at Station A from Station B can be modelled as

$$\boldsymbol{y_k^{UL}} = \boldsymbol{H_k^{UL} x_k^{UL}} + \boldsymbol{n_k} \tag{3.1}$$

$$\boldsymbol{H_k^{UL}} = \boldsymbol{D_{A,Rx,k} H_k D_{B,Tx,k}} \tag{3.2}$$

where y_kUL is the N_Ax1 signal vector arriving at Station A and $\boldsymbol{x_k^{UL}}$ is the N_Bx1 signal vector transmitted from Station B, all at subcarrier k. Also, n_k is a N_Ax1 matrix consisting of zero-mean complex IID AWGN noise with variance σ. Furthermore, $\boldsymbol{H_k^{UL}}$ is the combined N_AxN_B channel consisting of the reciprocal wireless channel H_k, Station B radio transmitter channel $\boldsymbol{D_{B,Tx,k}}$ and Station A radio receive channel $\boldsymbol{D_{A,Rx,k}}$. Station receives the uplink signal and proceeds to estimate the uplink channel $\boldsymbol{H_k^{UL}}$ using preambles and

pilot symbols. Depending on the transmission scheme, Station A will use the estimated uplink channel matrix to apply precoding.

Although the following assumes that zero-forcing precoding is the transmission of choice, it can be shown that other transmission schemes such as SVD decomposition for multiplexing and MRT for diversity all lead to the same conclusion. Station A uses the uplink channel estimate $\boldsymbol{H_k^{UL}}$ to precode the downlink signal $\boldsymbol{x_k^{DL}}$ with a linear precoding matrix $\boldsymbol{F_k^{DL}}$. The resulting downlink transmission is in the form

$$\boldsymbol{y_k^{DL}} = \boldsymbol{H_k^{DL} x_k^{DL} + n_k} \tag{3.3}$$

$$\boldsymbol{H_k^{DL}} = \boldsymbol{D_{B,Rx,k} H_k^T D_{A,Tx,k}} \tag{3.4}$$

where y_k^{DL} is the N_Bx1 signal vector arriving at Station B and $\boldsymbol{x_k^{DL}}$ is the N_Ax1 signal vector transmitted from Station A. Furthermore, $\boldsymbol{H_k^{DL}}$ is the combined N_BxN_A channel per subcarrier k consisting of the reciprocal wireless channel $\boldsymbol{H_k^T}$, Station A radio transmitter channel $\boldsymbol{D_{A,Tx,k}}$ and Station B radio receive channel $\boldsymbol{D_{B,Rx,k}}$. Ideally, for zero-forcing precoding, the precoding matrix $\boldsymbol{F^{DL}}$ is the matrix inversion of H^{UL}. When the downlink transmission equation is expanded, the following observation is made.

$$\boldsymbol{y^{DL}} = \boldsymbol{H^{DL} F^{DL} x^{DL} + n} \tag{3.5}$$

$$\boldsymbol{y^{DL}} = \boldsymbol{D_{B,Rx} H^T D_{A,Tx} (D_{A,Rx} H D_{B,Tx})^{-T} x^{DL} + n} \tag{3.6}$$

$$\boldsymbol{y^{DL}} = \boldsymbol{D_{B,Rx} H^T D_{A,Tx} D_{A,Rx}^{-1} H^{-T} D_{B,Tx}^{-1} x^{DL} + n} \tag{3.7}$$

$$\tag{3.8}$$

It is observed that the multiplication of $\boldsymbol{D_{A,Tx,k} D_{A,Rx,k}^{-1}}$ is imperative to the channel reci-

procity assumption. In order to minimize multi-user interference (MUI), the multiplication should result in a scalar constant multiplied by the identity matrix.

$$\boldsymbol{D_{A,Tx}D_{A,Rx}^{-1}} = \alpha * \boldsymbol{I_A} \tag{3.9}$$

Only through that relationship will MUI be prevented and the channel reciprocity assumption can hold. If this is achieved, then the diagonal matrices representing the transmit and receive RF chains $\boldsymbol{D_{B,Tx,k}}$ amd $\boldsymbol{D_{B,Rx,k}}$ of Station B have negligible effect on channel reciprocity and can be equalized at Station B.

3.1 Explicit Calibration

Explicit calibration consists of calibrating the transceiver radios of the CSIT-requiring station by using some combination of external loopback and a noise generator or calibration transmitter with a known training sequence. The calibration can be performed when the station is online or offline. Although there is some flexibility in how the calibration is performed, most calibration procedures for mitigating channel reciprocity involve the use of a calibration transmitter or transceiver, as well as either external loopback from the transmitter to receiver or splitters, couplers and combiners in junction with the antenna switches for enabling different configurations for measuring transceiver frequency response [6, 10, 18]. For loopback, the transmitter is connected to the receiver of each transceiver pair of the N_A radios.

With the transmitters loopbacked to the receivers, as shown in Figure (3.2), each transmitter can send a known training sequence across all OFDM subcarriers which will arrive

at the receivers of the same station. The overall N_AxN_A transceiver frequency response matrix $\boldsymbol{D_{A,TxRx}} = \boldsymbol{D_{A,Tx}}\boldsymbol{D_{A,Rx}}$ can be measured at the receiver per subcarrier and averaged to reduce the effect of noise. The transmitters are then decoupled from the receivers and the calibration noise generator is then connected to the receivers. From there the calibration noise generator sends a known sequence to all the receivers through a power splitter and the receiver can then calculate the N_AxN_A receiver frequency response matrix $\boldsymbol{D_{A,Rx}}$. Once these matrices are known, the calibration values of $\boldsymbol{D_{A,TxRx}}./\boldsymbol{D^2_{A,Rx}}$ can be calculated by an element-wise division and pre-compensated digitally per subcarrier at the transmitter before the IFFT block.

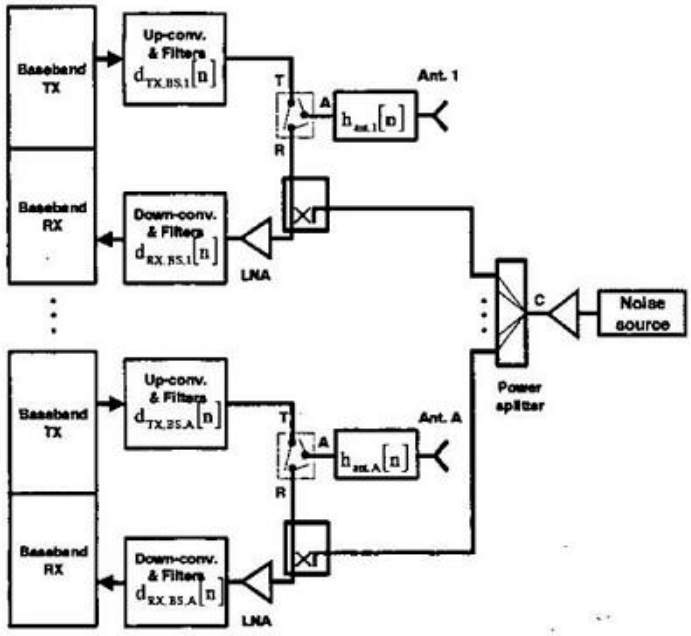

Figure 3.2: Explicit Calibration [6]

3.2 Implicit Calibration

Implicit calibration, as described in the 802.11n standard under implicit feedback [3], consists of the CSIT-requiring station calibrating itself by obtaining two sets of channel estimates. One set is obtained by using sounding, which means that it estimates the channel from uplink training sequences. The other set is obtained from quantized channel estimates that were calculated by the downlink station and embedded in the uplink frame. Using both sets of channel estimates, the CSIT-requiring station can then proceed to calculate correction factors that can be used to pre-compensate the transmitted data.

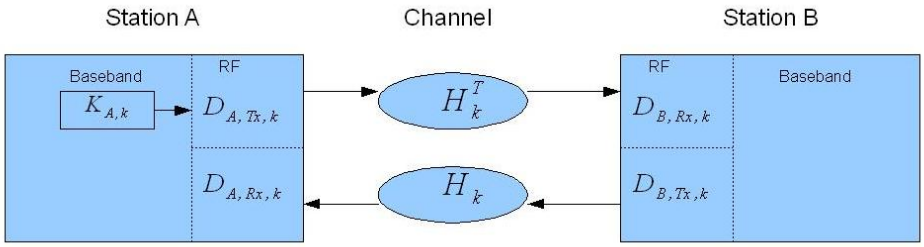

Figure 3.3: Equivalent Baseband-to-Baseband Channel with Correction Factor

Similar to Figure (3.1), Figure (3.3) shows the concatenated wireless channel plus radio channel between Station A and Station B. The exception is that a correction matrix $\boldsymbol{K_{A,k}}$ is added at Station A. The equivalent baseband-to-baseband channel can be expressed through the following equations.

$$\hat{\boldsymbol{H}_{\boldsymbol{AB,k}}} = \boldsymbol{D_{B,Rx,k}} \boldsymbol{H_{AB,k}} \boldsymbol{D_{A,Tx,k}} \tag{3.10}$$

$$\hat{\boldsymbol{H}_{\boldsymbol{BA,k}}} = \boldsymbol{D_{A,Rx,k}} \boldsymbol{H_{BA,k}} \boldsymbol{D_{B,Tx,k}} \tag{3.11}$$

The correction matrix $K_{A,k}$ must be computed such that reciprocity can be maintained in the equivalent baseband-to-baseband channel.

$$\hat{\boldsymbol{H}}_{\boldsymbol{AB,k}}\boldsymbol{K}_{\boldsymbol{A,k}} = \hat{\boldsymbol{H}}_{\boldsymbol{BA,k}}^{\boldsymbol{T}} \tag{3.12}$$

The correction matrix $\boldsymbol{K}_{\boldsymbol{A,k}}$ can be calculated in a variety of ways, the simplest being the complex division of $\boldsymbol{K}_{\boldsymbol{A,k}} = \hat{\boldsymbol{H}}_{\boldsymbol{BA,k}}^{\boldsymbol{T}} ./ \hat{\boldsymbol{H}}_{\boldsymbol{AB,k}}$ to derive the first set of correction factors. The correction matrix can be periodically updated based on the channel coherence time and other factors.

Chapter 4

Implementation, Measurements and Results

The validity of channel reciprocity within an OFDM wireless system needed to be tested a real-time hardware platform. In order to test channel reciprocity, the Wireless Open-Access Research Platform (WARP) provided by Rice University was utilized to conduct experiments. A description of the WARP system, as well as the actual experiment setup and results will be given in the rest of the chapter.

4.1 WARP System

The WARP system (WARP[1]) provides a real-time hardware prototyping environment for creating and testing wireless physical and MAC (Medium Access Control) layer algorithms. The main part of the system consists of a Xilinx Vitex2-Pro FPGA baseband development board in which the FPGA contains an embedded IBM PowerPC processor. The base-

band board also contains relevant components and I/O such as SDRAM, Ethernet, USB, RS232, Flash, and standard headers which enable form-factor daughterboards to interface directly with FPGA digital I/O. Signal processing algorithms are created using Xilinx System Generator in conjunction with MATLAB/Simulink and are targeted to the Xilinx Virtex2-Pro FPGA whereas MAC layer algorithms are constructed using Xilinx Embedded Development Kit (EDK) and are targeted to the embedded IBM PowerPC processor. Top-level connectivity is constructed using Xilinx EDK and synthesis is done using Xilinx Integrated Software Environment (ISE). Communication between the MAC and physical layers is achieved by a top-level Xilinx proprietary system bus that connects all peripheral cores to the processor, and in which physical-layer and other peripheral cores are accessible to the processor using memory-mapped I/O.

Other components in the Xilinx Vitex2-Pro FPGA baseband development board include memory, a dedicated 10/100Mb Ethernet interface, USB interface, RS232 interface and a Flash reader capable of reading Compact Flash (CF) cards. The Ethernet interface provides a high-speed network link between a Host PC and the FPGA, where UDP/IP sockets and applications can be created on the embedded processor using Xilinx software and Intellectual Property (IP). The USB interface provides JTAG and boundary scan access, whereas the RS232 interface chiefly serves to debug the software running on the embedded processor. The flash reader serves to load FPGA bitstreams and processor instruction code from the CF card to the FPGA, as an alternative to programming the FPGAs using JTAG.

Standard headers on the baseband board enable daughterboards to directly connect

[1]http://warp.rice.edu

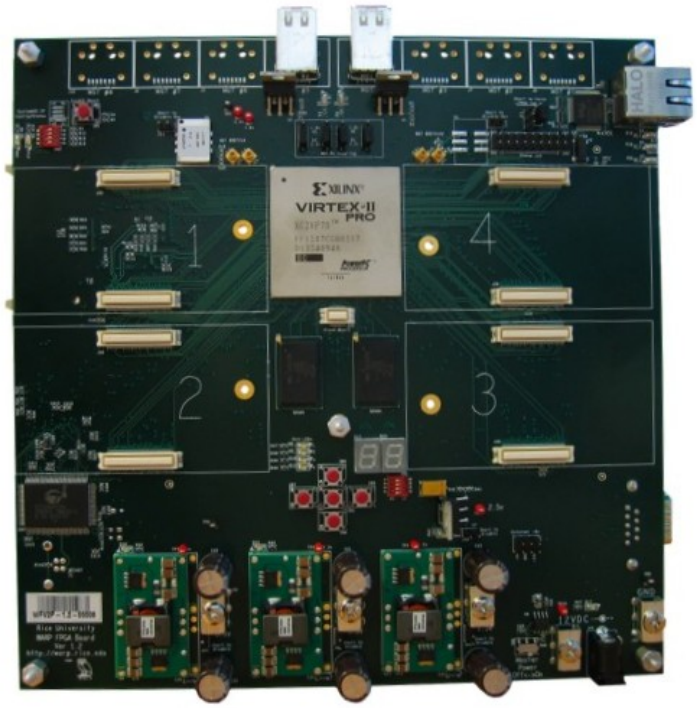

Figure 4.1: WARP Baseband Development Board

with FPGA I/O. Radio transceiver daughterboards were used to provide the Radio Frequency (RF) functionality needed for wireless transmission and reception. The radio transceiver board contains a AD9248 65MS/s 14-bit dual-ADC analog-to-digital converter (ADC), AD9777 160MS/s 16-bit dual digital-to-analog converter (DAC) and a AD9200 20MS/s 10-bit Receive Signal Strength Indicator (RSSI) chip all from Analog Devices. As well, a MAX2829 Maxim dual-band direct-conversion RF transceiver chip, Sharp IRM046U7 dual-band RF power amplifier designed to provide 18 dBm output power and DPDT RF switch are used for the RF front end. Some key features of the Maxim MAX2829 RF transceiver chip include: dual-band (2400-2500MHz, 4900-5875MHz), up to 40MHz bandwidth, analog I/Q Tx and Rx interfaces, 60dB RSSI range, 30dB Tx power control

range, 93dB Rx gain control range, and MIMO capable.

Figure 4.2: WARP Radio Board

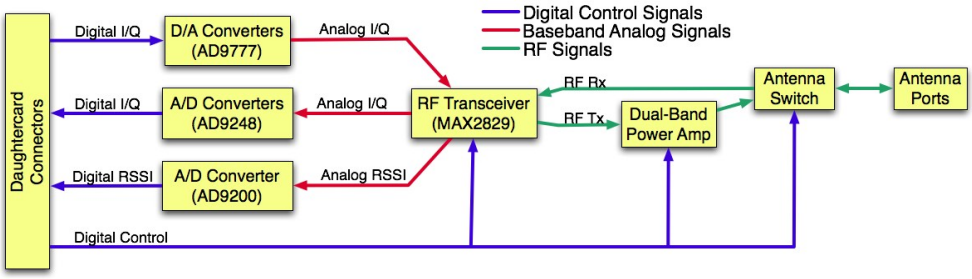

Figure 4.3: WARP Radio Block Diagram

4.1.1 OFDM Reference Design

Provided with the WARP development system is a reference design which loosely implements the IEEE 802.11a WiFi standard. The reference design comprises of a SISO-OFDM transmitter and receiver physical layer block on the FPGA and a Carrier Sense Multiple Access with Collision Avoidance (CSMA/CA) MAC on the processor. The reference design

acts as a wireless Ethernet bridge, essentially transmitting and receiving Ethernet frames over-the-air between two hosts which are each connected by Ethernet to the WARP boards [1].

The OFDM physical layer performs the functions illustrated in Figure (2.1). These include constellation mapping and IFFT at the transmitter, as well as timing/frequency offset estimation, channel estimation, equalization and demodulation at the receiver. The physical layer block runs at 40 MHz and is configurable through register access by the processor which is running at 160 MHz. The ADC and DAC are also clocked at 40 MHz and are synchronous to the OFDM physical layer core in the FPGA. The RF transceiver provides an over-the-air bandwidth of 10 MHz, which is a result of the 4x decimation and interpolation polyphase filters which are implemented in the OFDM core within the FPGA. The fixed modulation scheme per subcarrier is QPSK, the carrier frequency is fixed at channel 11 of the 2.4 GHz space and the transmit power at the output of the radio card is 18 dBm. A bandwidth of 10 MHz and a total of 64 subcarriers leads to a subcarrier spacing of

$$\triangle(f) = 10MHz/64 \tag{4.1}$$

$$\triangle(f) = 156.25kHz \tag{4.2}$$

This in turn leads to a total symbol period of

$$T_{tot} = T_s + T_{cp} \tag{4.3}$$

$$T_{tot} = T_s + 0.25T_s \tag{4.4}$$

$$T_{tot} = (1 + 0.25)/\triangle(f) \tag{4.5}$$

$$T_{tot} = 8\mu s \tag{4.6}$$

Of specific importance to the OFDM reference design is the packet structure, specifically the preamble and training fields, which are used to perform OFDM receive signal processing functions. The first part of the preamble field consist of 10 fixed sequences of 16 samples each, similar to the STS (Short Training Field) of the IEEE 802.11a standard. This part is used for Automatic Gain Control (AGC) and coarse timing synchronization. The second part of the preamble field consists of 2 fixed sequences of 64 samples each with an added 32 samples for CP, and is used for fine timing synchronization and coarse frequency offset estimation. The training field also uses 2 fixed sequences of 64 samples each with an added 32 samples for CP, similar to the Long Training Field (LTS) of the IEEE 802.11a standard. It is used for channel estimation and equalization for the duration of a packet which contains several OFDM symbols. Channel estimation is done in the frequency domain, and the estimates are averaged over the 2 sequences to reduce the effects of noise. Furthermore, pilot symbols are inserted within OFDM data symbols at fixed subcarriers for fine frequency tuning and phase noise tracking. The packet structure is shown in Figure (4.4).

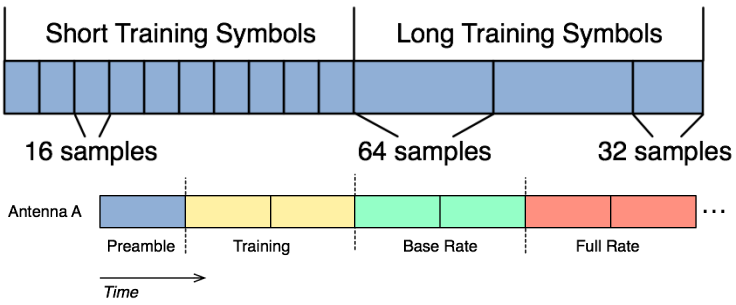

Figure 4.4: WARP Packet Structure

4.2 Implementation

In order to determine the validity of channel reciprocity in a real-time wireless hardware platform, a setup was needed that enabled the storage of consecutive real-time uplink and downlink channel estimates and centralization of the channel estimates for comparison and analysis. Though the OFDM reference design from Rice University provides for the OFDM physical layer needed to adequately estimate the channel, a method needed to be devised to store consecutive channel estimates in memory and process and compare the uplink and downlink channel estimates on a Host PC. Therefore the overall OFDM reference design, specifically the lack of memory for storing channel estimates, the unnecessary CSMA/CA MAC and the dependency of two Host PCs for wireless Ethernet transfer were deemed unacceptable.

The OFDM physical layer model was slightly modified to include a Xilinx Shared RAM memory module in the channel estimation block. Channel estimates can be stored every OFDM packet into the Shared RAM memory module. Before they are stored in memory, the channel estimates, per I and Q channel, are converted from signed 16-bit fixed-point representation to unsigned 16-bit integers. Furthermore, the memory is also attached to the

main processor system bus and is memory-mapped, meaning that the embedded processor can read the channel estimates from the shared memory.

The physical setup of the WARP reference design, with each WARP node connected by Ethernet to a PC, was not compatible to the idea of centralizing and processing the channel estimates into one Host PC. Therefore an Ethernet hub was used to connect one PC with two WARP nodes. Ethernet drivers and cores provided by Xilinx were used to program IP and MAC addresses to each WARP node, and UDP/IP sockets were instantiated within the embedded processor to allow for communication over the network. This was further complemented by drivers developed in MATLAB used to create UDP/IP sockets within MATLAB for communication with the WARP boards. In effect, channel estimates stored in the OFDM physical layer memory can be transferred to the embedded processor and eventually transmitted over the LAN into MATLAB running on the PC. Likewise, variable-size random packets can be created in MATLAB and transferred to both WARP nodes over the LAN where it is stored in the OFDM Tx buffer memory and eventually transmitted over-the-air.

The CSMA/CA MAC was not needed for the experiments since the main purpose of the experiments is to initiate bi-directional transfer between the two WARP nodes and reading in the channel estimates into MATLAB. Instead, a simple communication protocol loosely based on a framework developed by the WARP team at Rice University (WARPLAB) was created and developed to communicate between the Host PC and WARP boards. Commands issued from MATLAB were received and decoded by the destined WARP board. Based on the command, the destined WARP board would initiate such functions as storing the transmit data in memory, initiating OFDM transmission and retrieving channel

estimates from memory and transferring them over the LAN to MATLAB. Due to the long latency (700 ms) associated with transmission over the LAN, one OFDM transmission command sent from MATLAB to one board leads automatically to five consecutive back-and-forth OFDM transmissions between the two boards, leading to a total of five consecutive uplink and downlink channel estimate captures.

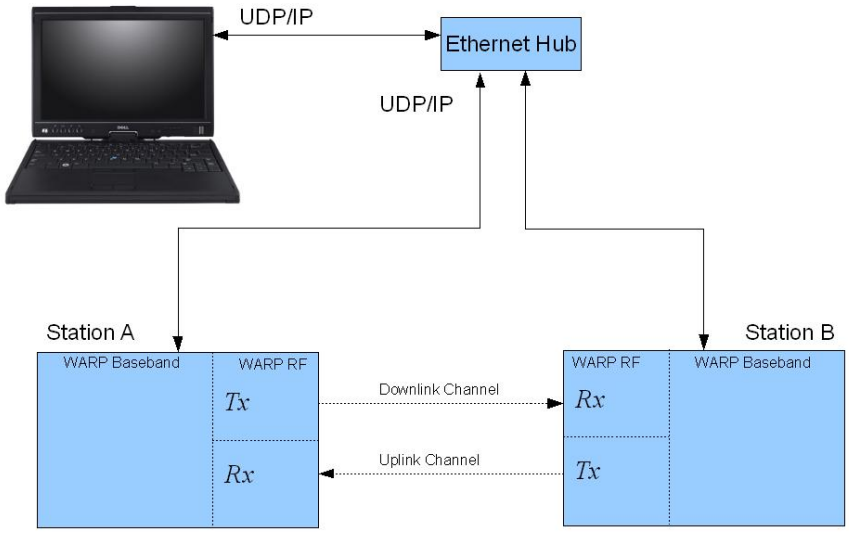

Figure 4.5: WARP Experiment Setup

4.3 Experiment Results

Using the WARP setup, experiments were conducted in which the antennas were located in a typical WiFi office setting and were distanced 2 meters apart within LOS (line-of-sight).

The uplink and downlink channel estimates were stored in real-time and then processed in MATLAB. The resulting frequency-domain channel magnitude and phase (in radians) for the 64 subcarriers are shown in Figure (4.6) for five consecutive bi-directional OFDM transmissions between the first radios of each board.

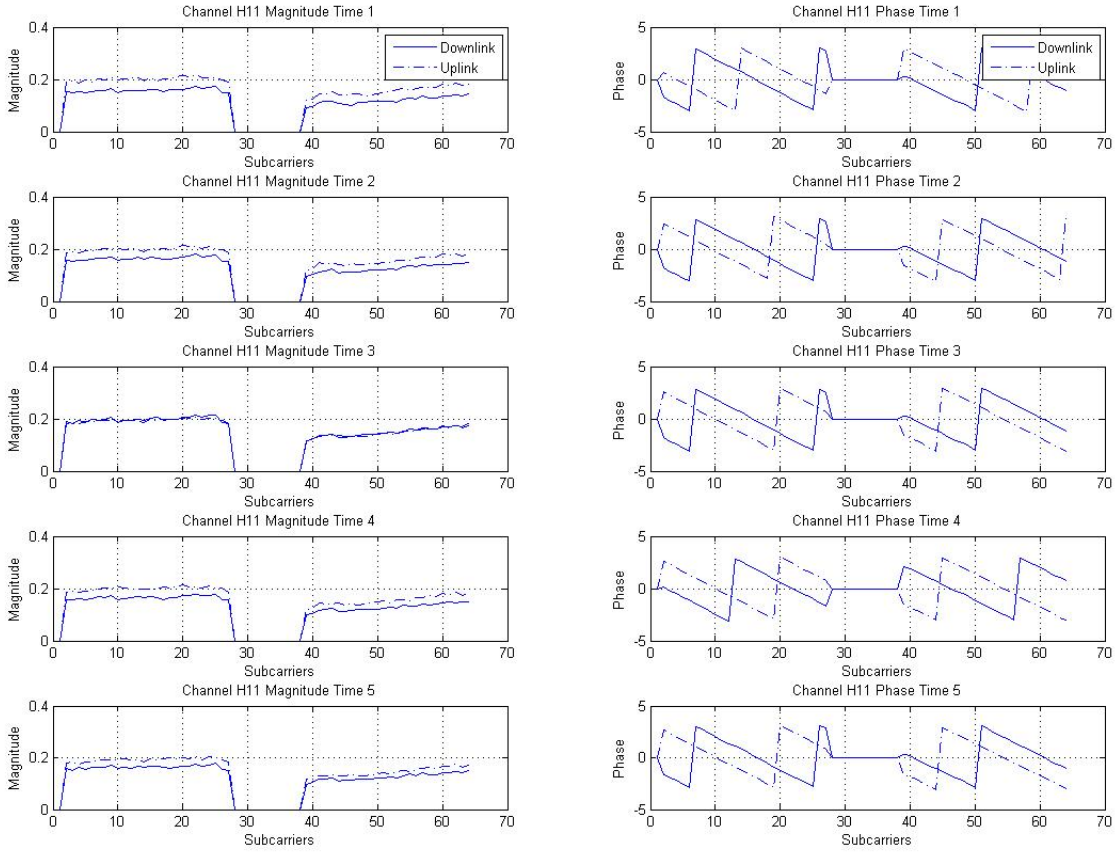

Figure 4.6: Channel Reciprocity Plots

4.3.1 Reciprocity for Channel Magnitude

The overall shape of the uplink and downlink channel magnitude plots for all five captures appear to be very similar in shape. Uplink and downlink magnitude fluctuations occur around the same subcarriers, and the actual magnitudes differ slightly. The overall shape of the uplink and downlink channel magnitude frequency response is more imperative for channel reciprocity than the magnitude values, since compensation can be achieved by a multiplicative scalar factor. It should be noted that the uplink and downlink channel magnitude plots do not reflect the true value of the channel magnitude, since the AGC and LNA influences the power level of the received signal. However, the channel magnitude shape does indeed reflect the magnitude response of the channel since the same components affect the gain at all subcarriers equally.

Applying linear compensation to maintain reciprocity consists of using the correction factor $\mid K_{A,k} \mid = \mid H_{BA,k} \mid ./ \mid H_{AB,k} \mid$ as expressed in Section (3.2). This correction factor, to be applied at Station A (uplink terminal), is illustrated in Figure (4.7) for all subcarriers.

The scalar correction factor is more or less constant across all subcarriers for all five captures, and they vary in value between the five captures from 0.8 to 1.1.

4.3.2 Reciprocity for Channel Phase

The uplink and downlink channel phase plots for all five captures in Figure (4.6) exhibit linear phase, which is customary for group delay. Though the uplink and downlink channel phase plots deviate from each other in phase by a few radians, the slope of both uplink and downlink channel phase plots are similar. This validates the reciprocity principle in the sense that the overall channel frequency phase for uplink and downlink exhibit the

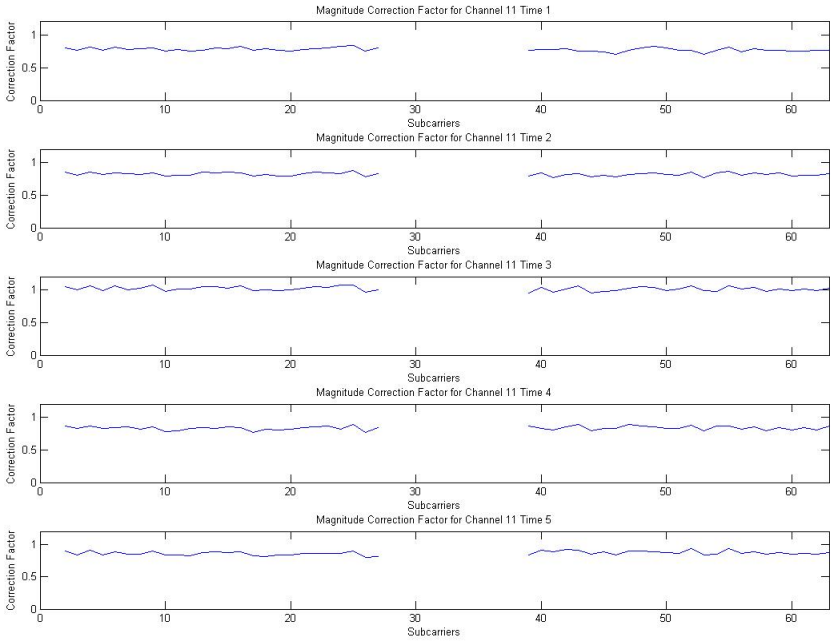

Figure 4.7: Magnitude Correction

same rate of change across subcarriers, which points to a similar uplink and downlink channel group delay. As explained in Section (2.2), phase differences between the uplink and channel phase plots can be attributed to RF front-end imperfections, namely carrier frequency offsets, timing offsets and sampling time deviations. Though the channel is considered stationary, the plots exhibit differing behaviour from capture to capture. One explanation for this is that the oscillators that are used to derive the carrier frequency and sampling clock undergo considerable drift across time, and that this drift inadvertantly affects the channel response.

Applying linear compensation to maintain reciprocity consists of applying a correction factor, which is obtained in a slightly different way than that of magnitude. Instead

a subtraction is used since dividing complex numbers is equivalent to subtracting their respective phases. The correction factor, to be applied at Station A in baseband before the IFFT, can be calculated as $\theta_{K_{A,k}} = \theta_{H_{BA,k}} - \theta_{H_{AB,k}}$ and is illustrated in Figure (4.8) for all subcarriers.

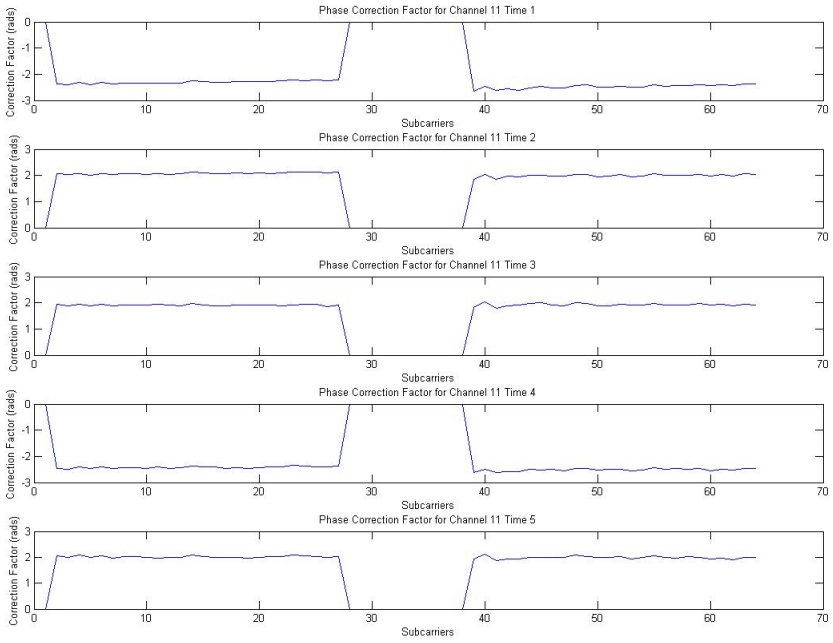

Figure 4.8: Phase Correction

The phase correction factor in each capture remains nearly constant across all subcarriers, which shows that the uplink and downlink channel exhibit the same group delay and characteristics. Discontinuities in the phase correction factors occurred because the channel phase is restricted to $[-\pi\pi]$, and these discontinuities were avoided by applying a 2π modulus operation.

Chapter 5

Conclusion and Future Work

Channel knowledge at the uplink terminal leads to higher throughput for SISO-OFDM wireless systems and increased capacity and diversity for MIMO-OFDM wireless systems, such as those described in the IEEE 802.11n standard and LTE. Algorithms that benefit from CSIT include AMC for higher throughput, MRT for increased diversity and SVD for increased capacity. For TDD systems specifically, channel knowledge at the uplink terminal can be obtained by assuming the downlink and uplink channel are reciprocal at no additional bandwidth cost.

However, there exists detriments to channel reciprocity that manifest themselves in CSIT errors and ultimately degrade performance. These include differing narrowband interference structures at the transmitter and receiver, mobile (receiver) speed in relation to OFDM symbol period and especially RF front-end imperfections. Specifically, RF front-end imperfections include carrier frequency deviations, timing offsets and sampling time deviations between the uplink and downlink terminal RF front-ends. These imperfections can be modelled as subcarrier-dependent multiplicative complex phase factors, and ulti-

mately influence the channel phase response more than the channel magnitude response.

Compensation for channel non-reciprocity generally consists of calibration to detemine the phase response of the RF transceiver circuitry, and precoding in baseband to compensate for the transceiver effects. Calibration can be done by two general methods: explicit calibration, in which loopback and external circuitry is used to calculate the transceiver response and implicit calibration, in which the uplink terminal obtains both its own channel uplink estimate and the channel downlink estimates from the downlink terminal and then applies linear correction factors for compensation. Implicit calibration is generally seen as a more efficient method since it doesn't require any additional hardware or loopback configuration.

Using a real-time wireless research hardware platform called WARP, experiments were conducted in which consecutive uplink and downlink channel estimates were collected and analyzed. Results have shown that the uplink and downlink channel magnitude responses are in fact reciprocal, and that scalar correction factors can be applied at baseband to compensate for amplitude differences. Even though uplink and channel channel phase responses deviate in phase they are reciprocal in slope and shape, exhibiting similar group delays. Phase deviations can be attributed to the RF transeiver imperfections mentioned earlier, and can be compensated by precoding the baseband signal with a complex phase equal to the actual phase deviation.

Future research in this area could be applied in implementing an actual AMC, MRT or SVD algorithm using the WARP platform. Performance comparisons can be made between these algorithms that actually use implicit calibration to derive and apply their correction factors at baseband and the same algorithms that do not attempt to compensate

for reciprocity. Also, performance comparisons can be made between algorithms that use implicit calibration for compensation and the same algorithms using explicit calibration.

References

[1] Rice university warp project (http://warp.rice.edu).

[2] IEEE Standard 802.11a 1999. *Wireless LAN Medium Access Control (MAC) and Physical Layer (PHY) Specifications: High-speed Physical Layer in the 5GHz Band*. IEEE, September 1999.

[3] IEEE Standard 802.11nD2.00 2007. *Wireless LAN Medium Access Control (MAC) and Physical Layer (PHY) Specifications: Enhancements for Higher Throughput*. IEEE, September 2007.

[4] IEEE Standard 802.16e 2005. *Local and Metropolitan Area Networks - Part 16, Air Interface for Fixed Broadband Wireless Access Systems*. IEEE, September 2005.

[5] G. Barriac and U. Madhow. Space-time communication for OFDM with implicit channel feedback. *IEEE Transactions on Information Theory*, 50(12):3111–3129, 2004.

[6] A. Bourdoux, B. Come, N. Khaled, I. DESICS, and B. Leuven. Non-reciprocal transceivers in OFDM/SDMA systems: Impact and mitigation. In *Radio and Wireless Conference, 2003. RAWCON'03. Proceedings*, pages 183–186, 2003.

[7] S. Catreux, V. Erceg, D. Gesbert, RW Heath Jr, I.W. Inc, and CA San Jose. Adaptive modulation and MIMO coding for broadband wireless datanetworks. *IEEE Communications Magazine*, 40(6):108–115, 2002.

[8] M. Codreanu, D. Tujcovic, and M. Latva-Aho. Adaptive MIMO-OFDM with low signalling overhead for unbalanced antenna systems. *IEICE Transactions on Communications*, pages 28–38, 2005.

[9] M. Codreanu, D. Tujkovic, and M. Latva-aho. Compensation of channel state estimation errors in adaptive MIMO-OFDM systems. In *2004 IEEE 60th Vehicular Technology Conference, 2004. VTC2004-Fall*, volume 3, 2004.

[10] AR Dias, D. Bateman, and K. Gosse. Impact of RF front-end impairments and mobility on channel reciprocity for closed-loop multiple antenna techniques. In *15th IEEE International Symposium on Personal, Indoor and Mobile Radio Communications, 2004. PIMRC 2004*, volume 2, 2004.

[11] S. W. McLanughln Y. Li M. A. Ingram G. L. Stuber, J. R. Barry and T. G. Pratt. Broadband mimo-ofdm wireless communications. *Proceedings of the IEEE*, 92(2), Feb. 2004.

[12] S. Georgoulis and DGM Cruickshank. Pre-equalisation, transmitter precoding and joint transmissiontechniques for time division duplex CDMA. In *3G Mobile Communication Technologies, 2001. Second International Conference on (Conf. Publ. No. 477)*, pages 257–261, 2001.

[13] M. Guillaud, D.T.M. Slock, and R. Knopp. A practical method for wireless channel

reciprocity exploitation through relative calibration. In *Proc. Eighth International Symposium on Signal Processing and Its Applications (ISSPA05),(Sydney, Australia)*. Citeseer, 2005.

[14] A. Hottinen. Channel reciprocity for fdd systems using duplex hopping. Technical Report AN3059, Nokia Research Center, 2004.

[15] M. Sandell S. K. Wilson J. J. van de Beek, O. Edfors and P. O. Borjesson. On channel estimation in OFDM systems. In *Proc. IEEE Vehicular Technology Conf.*, volume 2, pages 815–819, Chicago, IL., July 1995.

[16] G. Lebrun, J. Gao, and M. Faulkner. MIMO transmission over a time-varying channel using SVD. *IEEE Transactions on wireless Communications*, 4(2):757–764, 2005.

[17] G. Li and G.L. Stuber. *Orthogonal frequency division multiplexing for wireless communications*. Springer, 2006.

[18] J. Liu, A. Bourdoux, J. Craninckx, P. Wambacq, B. Come, S. Donnay, and A. Barel. OFDM-MIMO WLAN AP front-end gain and phase mismatch calibration.

[19] L. Liu and H. Jafarkhani. Successive transmit beamforming algorithms for multiple-antenna OFDM systems. *IEEE Transactions on Wireless Communications*, 6(4):1512–1522, 2007.

[20] J. J. van de Beek S. K. Wilson O. Edfors, M. Sandell and P. O. Borjesson. Ofdm channel estimation by singular value decomposition. *IEEE Trans. Commun.*, 46(7), July 1998.

[21] M. K. Ozdemir and H. Arslan. Channel estimation for wireless ofdm systems. *IEEE Commun. Surveys Tutorials*, 9(2), 2007.

[22] J. Proakis. *Digital Communications*. McGraw-Hill, 1989.

[23] J. Ran E. Bolinth R. Grunheid, H. Rohling and R. Kern. Robust channel estimation in wireless LANs for mobile environments. In *Proc. IEEE Vehicular Technology Conf. VTC 2002*, volume 3, pages 1545–1549, Sept. 2002.

[24] A. Tolli and M. Codreanu. Compensation of interference non-reciprocity in adaptive TDD MIMO-OFDM systems. In *15th IEEE International Symposium on Personal, Indoor and Mobile Radio Communications, 2004. PIMRC 2004*, volume 2, 2004.

[25] A. Tolli, M. Codreanu, and M. Juntti. Suppression of non-reciprocal interference in adaptive MIMO-OFDM cellular systems. In *2005 IEEE 61st Vehicular Technology Conference, 2005. VTC 2005-Spring*, volume 2.

[26] A. Tolli, M. Codreanu, and M. Juntti. System level impact of nonreciprocal interference in adaptive MIMO-OFDM cellular systems. *Proc. IST Mobile & Wireless Telecommun. Summit. Dresden, Germany*, 2005.

[27] K. H. Paik W. G. Jeon and Y. S. Cho. An efficient channel estimation technique for OFDM systems with transmitter diversity. In *Proc. IEEE Int'l. Symp. Personal, Indoor and Mobile Radio Commun.*, volume 2, pages 1246–1250, London, UK, Sept. 2000.

[28] M. Wouters, A. Bourdoux, S. Derore, S. Janssens, and V. Derudder. An Approach for Realtime Prototyping of MIMO-OFDM Systems.

[29] S. Wu and Y. Bar-Ness. OFDM channel estimation in the presence of frequency offset and phase noise. In *Proc. IEEE Int'l. Conf. Commun.*, pages 3366–70, May 2003.

[30] D. Zeng and R. Song. Elimination of Interference Non-Reciprocity in TDD MIMO-OFDM Systems. In *Wireless Communications, Networking and Mobile Computing, 2007. WiCom 2007. International Conference on*, pages 105–108, 2007.